EVIDENCE FOR LOCAL AND NONLOCAL BAROTROPIC RESPONSES TO ATMOSPHERIC FORCING DURING BEMPEX

Douglas S. Luther, Alan D. Chave[1], Jean H. Filloux, and Peter F. Spain

Scripps Institution of Oceanography

Abstract. The coherence between single bottom pressure and barotropic velocity records collected in the North Pacific during BEMPEX and air pressure, wind stress, and wind stress curl derived from FNOC products are examined over the 200-1 day period band. Strong coherence between the bottom pressure and all atmospheric variables is seen, with nonlocal coherence (maximum up to 1000 km to the southeast) dominating at periods longer than $\approx$10 d and local coherence being prevalent at shorter periods, consistent with predictions from existing models of atmospherically-forced barotropic motion. The azimuth of the nonlocal coherence maximum relative to the ocean station is a function of frequency, which is not expected from the models. The coherence between the barotropic velocity (as measured by the electric field) and the atmospheric variables is weaker, but nonlocal coherence with the wind stress and wind stress curl at periods greater than a week, and local coherence with the wind stress at shorter periods, is statistically significant.

Introduction

Much of the deep ocean's subinertial variability is probably due to depth-independent (barotropic) motions that are directly, atmospherically forced, except near regions dominated by the instabilities of mean currents. Stochastically-forced, viscid models of wind-forced flow [e.g., Müller and Frankignoul, 1981; hereafter referred to as MF] predict barotropic currents in a flat-bottomed basin that are coherent with local atmospheric variables only at periods short (<10 d) relative to those of free Rossby waves and at long periods (>100 d) where a Sverdrup balance obtains. The local coherences are small at intermediate periods due to decorrelation associated with the broad wavenumber bandwidth of the free Rossby waves. However, the lack of local coherence in any period band does not preclude significant nonlocal coherence between oceanic and atmospheric variables, as shown in model studies by Brink [1989] and Samelson [1989] (hereafter referred to as BR and SA). Evidence has been found for both local [Niiler and Koblinsky, 1985; Koblinsky et al., 1989] and nonlocal [BR] coherence between ocean currents and wind stress curl (hereafter simply curl), but attempts to model these observations have only been partially successful. This note adds to the growing body of evidence for

[1] also at AT&T Bell Laboratories, Murray Hill.

direct atmospheric forcing of deep ocean currents, while further spotlighting model strengths and weaknesses.

In 1986-7, a large (1000 km by 1000 km) array of seafloor pressure and electromagnetic data was collected in the North Pacific centered on 40°N, 163°W during the Barotropic ElectroMagnetic and Pressure EXperiment (BEMPEX) [Luther et al., 1987], in part to test assertions about atmospheric forcing of barotropic currents. Both horizontal electric field and bottom pressure data are inherently sensitive to barotropic fluctuations, filtering out most of the baroclinic component. The consistency of the observed horizontal electric field with theoretical predictions about its vertical averaging properties is demonstrated by Chave et al. [1990], so electric field measurements are treated as barotropic current estimates hereafter.

The seafloor data consist of 10-11 month records of pressure at site PC (40.7°N, 169.3°W) and vector horizontal electric field (barotropic currents) at site EB (40.6°N, 163.0°W); bathymetric maps of the BEMPEX area showing the instrument locations can be found in Luther et al. [1987]. The barotropic current (pressure) has a maximum deviation from the mean of 3 cm/s (22 mb) and a standard deviation about the mean under 1 cm/s (5 mb). Fluctuations of the surface air pressure and wind fields at 6 h intervals were obtained at 405 locations over the North Pacific from the Fleet Numerical Oceanographic Center. BR and others have demonstrated better consistency of the FNOC winds with direct observations than for other atmospheric products, justifying their use here. The wind velocity data were converted to wind stress estimates at 10 m using the Monin-Obukhov similarity formula and a velocity-dependent neutral drag coefficient. The curl was computed using a two-dimensional centered finite difference operator.

The two point coherence and phase between the oceanic variables and all 405 surface values of air pressure, zonal and meridional wind stress, and curl were computed in 23 overlapping period bands covering the 1-200 d range, yielding a large set of squared coherence and phase maps. Similar maps of the intercorrelations between the atmospheric data at reference sites in the BEMPEX area and the remaining atmospheric variables were also produced. In addition, frequency-wavenumber spectra of the atmospheric data were computed by the maximum likelihood method using a small number of stations centered on the BEMPEX area.

The wavenumber spectra of air pressure indicate an increasingly strong tendency toward eastward propagation as the period decreases below 10 d, in agreement with earlier studies. There are weak indications of westward propagation at longer periods and a slight northward component occurs at periods beyond 40 d. The zonal winds exhibit

increasingly strong northeastward propagation at periods shorter than 10 d and no preferred direction at longer periods. The meridional winds display eastward propagation at periods less than 14 d and no distinct direction at longer ones.

These qualitative impressions are confirmed by the coherence and phase maps of the entire FNOC data set relative to reference sites in the BEMPEX area. However, it is also evident that the atmospheric variables can be coherent with themselves over large, sometimes irregularly shaped, areas. For example, the air pressure field is significantly intercorrelated over 30° of latitude and 90° of longitude at 28 d period. The coherent zone shrinks by only about 30% as a period of 2 d is reached. The zonal or meridional wind stress is typically correlated over more than 2000 km even at the shortest periods. The curl displays smaller correlation scales and disjoint regions of significant coherence, reflecting either complex atmospheric teleconnections, accentuation of short spatial scale components, a rise in the noise level, or a combination of these.

The existence of preferred propagation directions and large scale coherence for the atmospheric variables has two implications. First, at periods where the atmospheric variables show eastward phase propagation, a forced oceanic response that has no freely propagating wave characteristics may dominate even if free Rossby waves exist. This suggests that higher local coherences between oceanic and atmospheric variables may be seen in the field than are predicted by MF, who assumed a symmetric wavenumber spectrum for the forcing that results in more energy input at the wavelengths of free Rossby waves. Second, significant coherence between the oceanic and atmospheric variables over large (sometimes disjoint) areas complicates interpretation since it can be due either to a real extended relationship between the ocean and atmosphere or to a smaller scale ocean-atmosphere connection combined with intercorrelations of the atmospheric variables among themselves. The occurrence of irregularly shaped or disjoint regions of high ocean-atmosphere coherence cannot be explained by existing models [e.g., BR and SA] which employ smooth bottoms and simple parameterizations of the forcing.

Evidence for Atmospheric Forcing

While the principal mechanism for atmospheric forcing of large scale barotropic motions at the periods of interest is expected to be curl-generated Ekman pumping, the complete forcing function involves additional combinations of air pressure and wind stress [e.g., Philander, 1978]. Furthermore, since the FNOC products are approximations, and differencing accentuates noise in the curl, it seems prudent to explore the relationships between the oceanic data and all the surface atmospheric variables, not just curl.

Figure 1 shows the squared coherence and phase of the bottom pressure at PC with the air pressure in the 28 (40-21) and 2 (2.3-1.8) day bands. At 28 d, there is only marginal local coherence, but an extended, strongly coherent patch exists to the southeast, peaking ≈1000 km away. The weaker coherence to the northwest coincides with an extended region of air pressure intercorrelation, suggesting no direct causal relationship between the ocean and atmo-
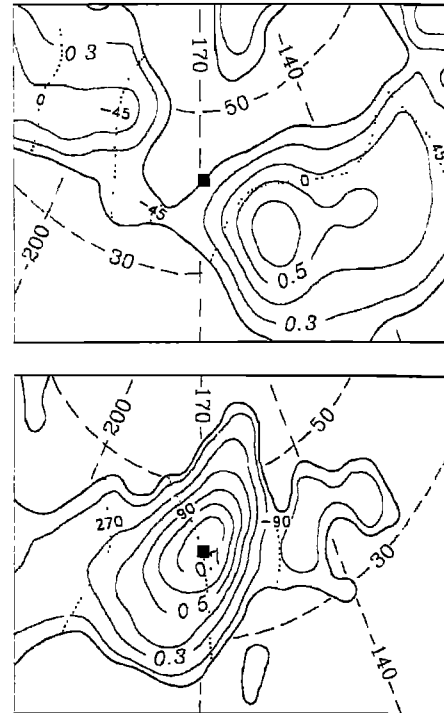

Fig. 1. Squared coherence maps between the bottom pressure at site PC (solid square) and 405 sites of FNOC atmospheric pressure observations at 28 d (top) and 2 d (bottom). The 405 FNOC grid points are evenly distributed over the polar stereographic domain shown. Only coherences statistically greater than zero at the 95% level are contoured; these values are 0.22 and 0.15 at the two periods, respectively. Selected north latitude and west longitude lines are shown dashed, while a few contours of the phase in the coherent regions are given as dotted lines. A positive phase means the atmospheric variable leads the oceanic one.

sphere there. MF predict negligible local squared coherence at a phase of 0° for this period. (NB, the phase convention in MF is opposite to that used here and will be changed in sign for further comparisons.) The observed local squared coherence barely exceeds the zero significance level at 95% confidence, and the observed phase of ≈-35° is not significantly different from the model value. Weak local coherence between bottom and air pressure is seen at periods longer than 23 d at this site with the peak coherence located to the south or southeast as in Figure 1 (top). From 17-14 d there is only nonlocal coherence peaking about 1000 km to the east. The spatial coherence patterns bear a qualitative resemblance to the correlation patterns of the air pressure with itself throughout the 200-14 d band. Local coherence is well-established at 12 d with the peak value occurring ≈1000 km to the east. With decreasing period, the patch becomes more centered on the station, as at 2 d in Figure 1 (bottom) where the coherence maximum is located at the seafloor instrument. The phase progression is consistent with a forced response to the generally eastward propagating atmospheric fields. The local squared coherence of ≈0.8 is considerably higher than the 0.14 predicted by MF, but the phase of ≈90° is similar to
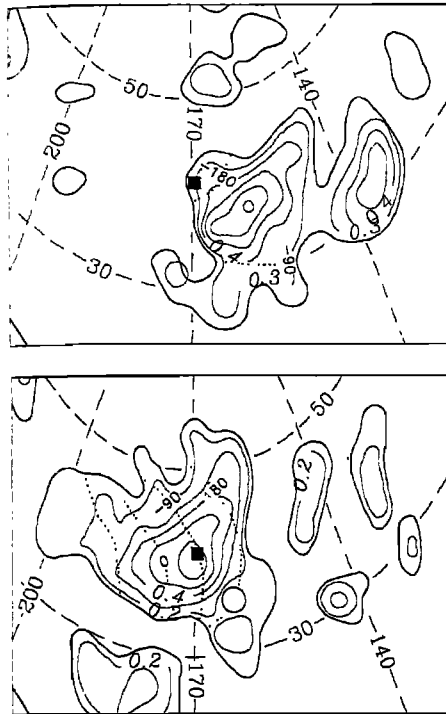
Fig. 2. Squared coherence maps between the bottom pressure at site PC and the curl at 28 d (top) and 2 d (bottom). The dotted phase contours are at 90° intervals. See Figure 1 caption for other details.

the model value. Local coherence with the air pressure remains high to 1.6 d period.

Figure 2 compares the coherence between the bottom pressure and the curl. At 28 d (top), there is weak local coherence with the highest values existing ≈600 km to the southeast. MF predict a negligible local coherence as compared to the ≈0.3 (0.08 above the 95% significance level) that is seen. The observed local phase is in approximate agreement with the model. The flat-bottomed simulation of BR predicts that the maximum coherence between bottom pressure and curl should occur due east of the pressure station. Extrapolating the model to the BEMPEX area with its weak large scale bottom slope (shallower to the north-northeast) suggests that the maximum coherence should be east-southeast along f/H contours, in rough agreement with the plot. The easternmost lobe in Figure 2 (top) corresponds to an intercorrelation of the curl, and may not reflect a direct physical relationship between the oceanic and atmospheric variables at that location. A different sequence of variation with period is observed for the bottom pressure versus curl coherence than versus air pressure. At very long periods there is marginal local coherence between bottom pressure and curl but strong nonlocal patches of correlation exist to the north and south of the bottom station. Local coherence is clearly established at 36 d with a pattern similar to that in Figure 2 (top) continuing to about 17 d period. Local coherence vanishes at that point but strong nonlocal coherence to the north and southeast is established that becomes more tenuous as period decreases. The BR and SA models do not exhibit this frequency dependence of the azimuth of the nonlocal

coherence relative to the oceanic instrument location. Weak local coherence reappears at 6 d with the bottom station located at the west end of the coherent patch; as period decreases the coherent patch migrates to the west and is centered over the bottom instrument below ≈4 d. At 2 d (Figure 2, bottom) the local squared coherence is about 0.6, much larger than MF predict, while the observed phase is ≈-90°, in agreement with MF.

Both the spatial coherence patterns and the coherence magnitudes are quite consistent among the five BEMPEX bottom pressure sites. A larger amount of variability is seen among the seven electric field (barotropic current) sites, probably reflecting both topographic influences and the higher wavenumber content of velocity measurements. The EB data used below are intended to illustrate atmospheric forcing effects in the barotropic velocity field without being comprehensive.

Coherence maps for meridional and zonal barotropic currents versus curl in the 28 (40-21) d band are shown in Figure 3. There is significant nonlocal coherence both to the northeast and to the south and southeast with peak values of up to 0.5. The patterns do not reflect intercorrelation of the curl. The result for the zonal current is consistent with BR's model prediction of two coherence maxima located symmetrically to the east of the ocean observations, especially if that prediction is extrapolated to the gentle slope of the BEMPEX area so that the axis of symmetry becomes east-southeast along an f/H contour. However, the result for the meridional current in Figure 3 (top) does not agree at all with the model prediction of only local coherence. The similarity of the top and bottom
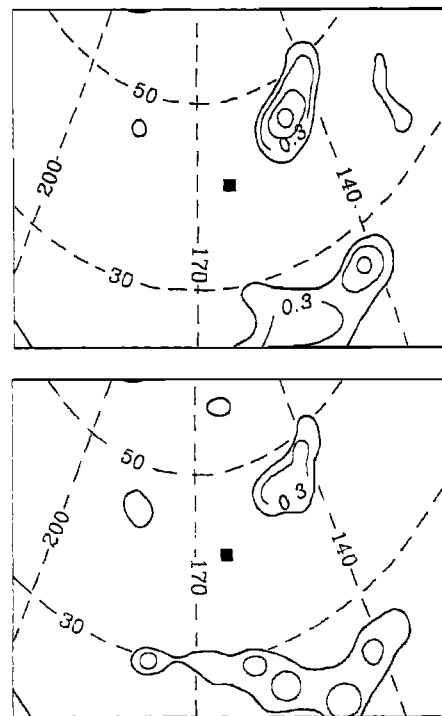

Fig. 3. Squared coherence maps between the meridional (top) and zonal (bottom) barotropic currents at EB and the curl at a period of 28 d. Only values exceeding the zero significance level of 0.22 at 95% confidence are included. See Figure 1 caption for other details.

frames of Figure 3 is consistent with the observed cyclonic polarization of the barotropic currents in this period band. The coherence patterns in Figure 3 persist throughout the 59-18 d band. At shorter periods, the coherence is generally weaker, nonlocal, and spatially scattered.

Figure 4 compares coherence maps of meridional velocity versus meridional wind stress at 6 (6.6-5.5) d (top) and zonal velocity versus zonal wind stress at 4 (4.6-3.6) d (bottom). There is local coherence in both instances. The observed squared coherences of ≈0.3 are smaller than the MF predictions of ≈0.6, but the phases are consistent with the model. The coherence patterns for barotropic velocity versus wind stress are more variable with period as compared to seafloor pressure, and will be discussed elsewhere.

While important similarities exist between these observations and the wind-forced models of MF (which provides local predictions) and BR and SA (which add nonlocal predictions), significant differences remain. The local coherences between the bottom pressure and all of the atmospheric variables are much higher (by up to a factor of four) than predicted by MF, although the phases are in approximate agreement. Reasonable phase agreement is seen for the barotropic velocity coherences with wind stress in Figure 4, but the squared coherences remain smaller than

the model values. Since the pressure field is sensitive to larger scale phenomena than the velocity field, the bigger observed pressure coherences suggest that there are fewer large scale Rossby waves in the real ocean than in the model, while the weaker observed velocity coherences indicate that smaller scale waves are either excited more or damped less than in the model. Similarly, the observed coherences between the atmospheric variables and both bottom pressure and barotropic velocity are larger than the model predictions of BR or SA. Significant pattern differences exist as well; in particular, the azimuth of the nonlocal coherence maximum is a strong function of frequency in the observations while it is constant in the models. A more quantitative comparison, for contrasting energy levels as well as coherences, requires that these models be run using topographic and curl data which are more appropriate for the North Pacific. Further clues to the discrepancies between observations and models may come from examination of the coherence pattern differences among the seven electric field sites in BEMPEX.

References

Brink, K.H., Evidence for wind-driven current fluctuations in the western North Atlantic, J. Geophys. Res., 94, 2029-2044, 1989.

Chave, A.D., D.S. Luther, and J.H. Filloux, Spatially-averaged velocity from the seafloor horizontal electric field, Proc. IEEE Fourth Work. Conf. Current Meas., in press, 1990.

Koblinsky, C.J., P.P. Niiler, and W.J. Schmitz, Jr., Observations of wind-forced deep ocean currents in the North Pacific, J. Geophys. Res., 94, 10773-10790, 1989.

Luther, D.S., A.D. Chave, and J.H. Filloux, BEMPEX: a study of barotropic ocean currents and lithospheric electrical conductivity, EOS, 68, 618-619, 628-629, 1987.

Müller, P., and C. Frankignoul, Direct atmospheric forcing of geostrophic eddies, J. Phys. Ocean., 11, 287-308, 1981.

Niiler, P.P., and C.J. Koblinsky, A local time-dependent Sverdrup balance in the eastern North Pacific Ocean, Science, 229, 754-756, 1985.

Philander, S.G.H., Forced oceanic waves, Rev. Geophys., 16, 15-46, 1978.

Samelson, R.M., Stochastically forced current fluctuations in vertical shear and over topography, J. Geophys. Res., 94, 8207-8215, 1989.
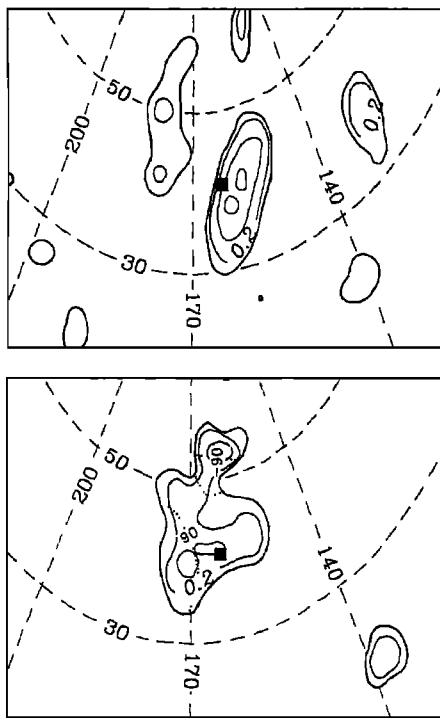

Fig. 4. Squared coherence maps between the meridional barotropic velocity at EB and meridional wind stress at 6 d (top) and zonal barotropic velocity at EB and zonal wind stress at 4 d (bottom). Only values exceeding the zero significance level of 0.15 at 95% confidence are included. See Figure 1 caption for other details. A few contours of the phase lead of the atmospheric over the oceanic variable are shown dotted at the bottom; the phase is 80°±10° in the central coherent region for the top panel.

A.D. Chave, AT&T Bell Laboratories, 600 Mountain Ave., Murray Hill, NJ 07974

J.H. Filloux, D.S. Luther, and P.F. Spain, Scripps Institution of Oceanography, La Jolla, CA 92093